Nonlinear Evolution of Stimulated Scatter in High-Temperature Plasmas

A. B. Langdon and D. E. Hinkel
Lawrence Livermore National Laboratory, Livermore, California 94550
(Received 6 December 2001; published 13 June 2002)

Simulations of laser-plasma interactions show saturation of Raman scattering through novel subsequent Brillouin and Raman rescattering instabilities. This behavior alters the interpretation of experimental diagnostics as well as the distribution of laser energy between transmission into the target, scattering losses, and generation of energetic electrons. This paper emphasizes targets that are predicted to reach electron temperatures greater than 10 keV, a value accessible today on the Omega and Helen lasers and one which will be far higher at future facilities. In such plasmas, the nonlinear laser-plasma interaction exhibits novel features presented here.

DOI: 10.1103/PhysRevLett.89.015003 PACS numbers: 52.38.Bv, 52.38.Dx, 52.38.Kd

Advances in the field of high energy density science (HEDS) require understanding energy loss mechanisms from an intense laser propagating through dense, high-temperature plasma. Of particular importance is stimulated backscatter by parametric instabilities, where light incident on such plasma backscatters off high-frequency electron plasma waves (stimulated Raman backscatter, SRBS) or off low-frequency ion acoustic waves (stimulated Brillouin backscatter, SBBS). Analysis of SRBS and SBBS of intense lasers in hot, dense plasma brings to light new saturation mechanisms that further our scientific understanding and are of academic interest.

Laser-target interactions have historically emphasized plasma conditions where the electron density $n_e \leq 0.1 n_c$ (n_c is the critical density where the incident light is reflected) and the electron temperature $T_e \leq 5$ keV. In this regime, both SBBS and SRBS have been extensively analyzed [1] for incident light with intensities ranging from low (where scattering is nominal) to relativistic levels.

The advent of more energetic lasers has and will continue to provide routine access to hotter, denser plasmas. The Omega laser at the Laboratory for Laser Energetics and the Helen laser at the Atomic Weapons Establishment both operate in this regime, as will the National Ignition Facility at the University of California Lawrence Livermore National Laboratory (LLNL) and the Laser Megajoule in France, currently under construction. In particular, these lasers have been and will be interacting with plasmas where $T_e \geq 10$ keV and $n_e \geq 0.1 n_c$, i.e., the HEDS regime.

To our knowledge there is not an analysis including both collective electron and ion effects of the nonlinear evolution of stimulated scatter interactions in this "frontier" regime. Estabrook and Kruer [2] concentrated on high-frequency electron waves in their analysis of the competition between SRBS and stimulated Raman forward scatter (SRFS), where an incident wave forward scatters off an electron plasma wave. They found that the growth rate for SRFS is comparable to that of SRBS for $n_e = 0.2 n_c$ and $T_e = 10$ keV with $v_0/c = 0.085$, where v_0 is the quiver velocity of an electron in the electric field of the laser and c is the speed of light.

We report here nonlinear evolution of stimulated scatter by successive rescattering instabilities. In particular, we show the first simulations where stimulated Brillouin backscatter of Raman forward-scattered light is identified [3]. In this process, the light wave created by Raman forward scatter, down-shifted in both frequency and wave number, scatters off an ion acoustic wave into a backward-propagating light wave. For these stimulated interactions, both frequency and wave number matching must occur, i.e., $\omega_0 = \omega_1 + \omega_{epw,iaw}$, $k_0 = k_1 + k_{epw,iaw}$. Here, $[(\omega_0, k_0), (\omega_1, k_1), (\omega_{epw}, k_{epw}), (\omega_{iaw}, k_{iaw})]$ are the frequency and wave number of the incident, scattered, electron plasma, and ion acoustic waves, respectively. Raman backscatter of the Raman forward-scattered light occurs at densities low enough for wave number matching to take place. Successive rescattering is a relevant mechanism for energy loss, as in our simulations SRFS is so vigorous that it depletes the incident laser light.

Rescattering of SRFS light by SBBS limits the growth of the waves associated with SRFS. As a consequence, the Langmuir waves will be smaller in amplitude and therefore will not trap as many electrons nor accelerate them to as high an energy. Rescatter will also result in less energy propagating in the forward direction, thereby reducing the efficiency of laser-driven systems. Finally, rescattering of SRFS light can affect the interpretation of backscatter spectra, where a spectral line associated with rescatter may be attributed to SRBS at lower density.

Rescatter of SRFS light by SBBS is a different saturation mechanism than found for plasma conditions where $n_e/n_c \sim 0.1$ and $T_e \sim 5$ keV. Such plasma parameters are typical of ignition regime conditions for inertial confinement fusion [4]. In the ignition regime we find that SRFS is limited by the Langmuir decay instability (LDI), where the Langmuir wave associated with SRFS decays into a backward Langmuir wave and a forward ion acoustic wave. This mechanism has been reported previously [5,6]. Both SRBS and SBBS of the incident light occur

in this regime as well. For these parameters, we also see evidence of rescatter of SRFS by SRBS.

It has been previously shown [6] that the condition for sufficient growth of LDI requires that as $k_{epw}\lambda_{de}$ increases [where k_{epw} is the wave number of the primary Langmuir wave, $\lambda_{de} \equiv [T_e/(4\pi n_e e^2)]^{1/2}$ is the electron Debye length, and e represents the electronic charge], the laser intensity must also increase. Thus as the electron temperature is increased for fixed laser intensity, saturation by LDI becomes less relevant. In this Letter, we find that high electron temperature plasmas favor saturation by mechanisms such as rescatter over LDI.

Plasma conditions, where $T_e \geq 10$ keV and $n_e/n_c \geq 0.1$, arise in a variety of HEDS experiments, where intense lasers create a high radiation temperature environment. To address the kinetic effects associated with backscatter in this regime, we performed a suite of one-dimensional (1D) particle-in-cell (PIC) simulations using Zohar [7]. Although SRBS is highly damped in this regime ($k_L\lambda_{de} > 0.3$, where k_L is the wave number of the Langmuir wave) it is still present, and there is significant SRFS as well ($k_L\lambda_{de} > 0.15$).

For these 1D simulations, the intensities are $0.25-1 \times 10^{16}$ W/cm^2 at wavelength 351 nm ($v_0/c = 0.015-0.03$). This is representative of intensities found in unsmoothed beams at the Omega and Helen lasers. Typically, these lasers have hot spots with a peak intensity in excess of 1×10^{17} W/cm^2. The electron temperature T_e ranges from 3 to 20 keV, with $ZT_e/T_i = 14$. The plasma density is $n_e/n_c = 0.2$, and the length of the simulated plasma is 100 micrometers. The higher electron temperatures approximate the conditions of targets in this HEDS regime.

We begin with $T_e = 3$ keV, $n_e = 0.2n_c$ and, at a reduced intensity, $I = 2.5 \times 10^{15}$ W/cm^2. Figure 1 is a plot of the light intensity normalized to the incident intensity in two different frequency bands vs normalized time, $\omega_0 t$. In this simulation, the Bohm-Gross shift between the forward and backward Raman light is indistinguishable. As T_e is increased, the frequency shift between forward and backscatter increases, and the two can be differentiated in frequency space. Here, however, that is not the case.

The bottom panel is a plot of the incident light (red) and the SBBS light (blue) in the frequency band $0.95 \leq \omega/\omega_0 \leq 1.05$. The middle panel depicts the forward-propagating light, i.e., the SRFS light (red) in the frequency band $0.40 \leq \omega/\omega_0 \leq 0.60$. In the top panel, we show the backward-propagating light in the same frequency band, i.e., the SRBS light (blue). Raman backscatter occurs in subpicosecond bursts centered about a normalized frequency $\omega/\omega_0 \sim 0.53$. After $\omega_0 t \sim 7000$, SRBS occurs at a reduced level. This decrement in SRBS, with a Langmuir wave number $k_L \sim 1.2(\omega_0/c)$, is accompanied by ion acoustic wave growth at wave number $k_{\text{ion}} \sim 2.3(\omega_0/c)$. This is saturation of SRBS by LDI [5,6], with wave number matching at $k_L = k_{\text{ion}} - k_L$. Raman forward scatter occurs at a level less than 5%,

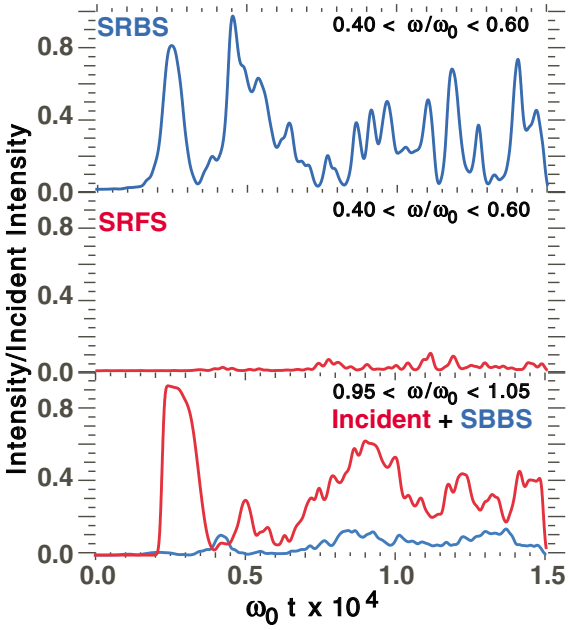

FIG. 1 (color). Normalized intensity vs $\omega_0 t$ for $T_e = 3$ keV, $n_e/n_c = 0.2$, and $I = 2.5 \times 10^{15}$ W/cm^2. The lower panel depicts the incident (red) and SBBS (blue) intensities, the middle panel depicts the SRFS intensity, and the upper panel depicts the SRBS intensity.

as does SBBS. The incident pump is not depleted in this simulation.

As the electron temperature is increased, interesting changes occur. Figure 2 is a plot of normalized light intensity vs $\omega_0 t$ in three different frequency bands which separate the incident and SBBS light from the SRFS light, and the SRFS light from the SRBS light. Here, $T_e = 20$ keV and $I = 1 \times 10^{16}$ W/cm^2 with $n_e/n_c = 0.2$. The bottom panel is the light intensity in the frequency band $0.95 \leq \omega/\omega_0 \leq 1.05$, encompassing the incident (red) and the SBBS light (blue). Here, SBBS is negligible, and the incident light is depleted by parametric processes by time $\omega_0 t \sim 3000$. The middle panel depicts light intensity in the frequency band $0.505 \leq \omega/\omega_0 \leq 0.60$, which includes the SRFS light, shown in red. There is also backward-propagating light in this frequency band, shown in blue. This is *not* the light associated with SRBS, which is plotted in blue in the top panel (frequency band $0.42 \leq \omega/\omega_0 \leq 0.505$). Rather, this backward-propagating light is the Brillouin backscatter of the forward Raman scattered light, i.e., SRFS is limited by rescatter. In this regime, the SRBS is heavily Landau damped, and SRFS is the primary parametric decay process [2]. The SRFS wave is prohibited from further decay by SRBS because the density is too high.

The spatial spectra of the waves provide supporting evidence. Early in time, at $\omega_0 t \sim 4000$ (*before* rescatter appears in the middle panel of Fig. 2), the primary feature in the electron spatial spectrum occurs at $k_L = 0.6(\omega_0/c)$,

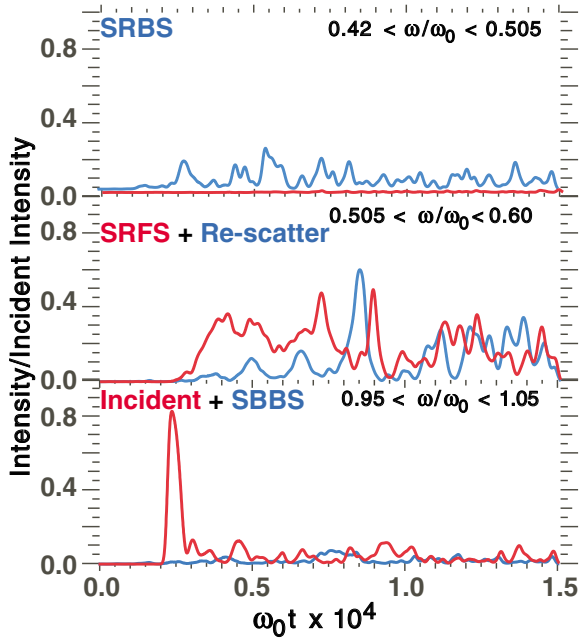

FIG. 2 (color). Normalized intensity vs $\omega_0 t$ in three frequency bands for $T_e = 20$ keV, $n_e/n_c = 0.2$, and $I = 1 \times 10^{16}$ W/cm^2. Incident (red) and SBBS (blue) intensities are depicted in the lower panel, SRFS light (red) and *rescatter* of SRFS by SBBS (blue) are depicted in the middle panel, and SRBS light (blue) is depicted in the top panel.

the wave number of the SRFS Langmuir wave. The incident wave has a wave number $k_{\rm inc} = 0.9(\omega_0/c)$, and the back- and forward-scattered electromagnetic waves both have a wave number magnitude $k_{sc} = 0.3(\omega_0/c)$. Wave number matching occurs for SRFS ($k_{\rm inc} = k_L + k_{sc}$).

Later in time, at $\omega_0 t = 12\,000$ (*after* rescatter appears in the middle panel of Fig. 2), the primary ion feature occurs at $k_{\rm ion} = 0.6(\omega_0/c)$, the primary electron feature at $k_L = 0.6(\omega_0/c)$, and the forward- and backscattered electromagnetic waves have wave number magnitude $k_{sc} = 0.3(\omega_0/c)$. Wave number matching, necessary for parametric processes, occurs when the forward-scattered electromagnetic wave backscatters off an ion wave ($k_{sc} = k_{\rm ion} - k_{sc}$). For these parameters, SRFS depletes the incident light, and then SBBS of the forward electromagnetic wave associated with SRFS occurs [8].

To isolate high-frequency scattering, we perform similar simulations except with immobile ions. For fixed ions, at $T_e = 20$ keV, the backward-propagating light in the middle panel of Fig. 2 disappears. In such simulations, SRFS is the dominant scattering process [2].

If we suppress SRFS by introducing a large enough density gradient, and allow the ions to move, the rescatter (blue) in the middle panel of Fig. 2 is again not present. Thus, by removing either the pump for this parametric process (no SRFS with a large enough density gradient) or the rescattering mechanism (by fixing the ions) the rescatter disappears. These simulations further substantiate our results.

We have also examined modifications to the electron distribution function in this HEDS regime. Figure 3 summarizes our findings, where we plot the fraction of electrons at energies above $E_e/(m_e c^2)$, the electron energy normalized to its rest mass energy, vs $E_e/(m_e c^2)$. We find that rescatter of the Raman forward-scattered light reduces the tail temperature *as well as* the number of hot electrons because it reduces the Langmuir wave amplitude. For fixed ions, where SBBS cannot deplete the SRFS light, the tail of the distribution function is at a temperature of about 210 keV. For mobile ions the tail temperature is reduced to 165 keV. Also, the hot electron fraction is reduced by a factor of 5 for energies above 500 keV when the ions are mobile.

In this regime, hot electrons are primarily generated through particle trapping in the Langmuir wave associated with SRFS ($v_{ph} \sim 4.5 v_e$). The third curve of Fig. 3 is a plot of the distribution function when SRFS is suppressed by introducing a density gradient. Hot electrons are then generated by particle trapping in the Langmuir wave associated with SRBS, which has a phase velocity down in the bulk of the distribution function at $v_{ph} \sim 2.7 v_e$. When SRFS is suppressed, electrons are not accelerated to as high an energy, and the tail temperature is reduced to about 47 keV, as expected.

We have also performed PIC simulations in the ignition regime, with $T_e = 5$ keV and $n_e/n_c = 0.1$. In Fig. 4 the dashed curves depict the fixed ion simulation, and the solid curves depict the mobile ion simulation. The lower panel is a plot of intensity in the frequency band $0.95 \le \omega/\omega_0 \le 1.05$, which includes the incident light (red) and the SBBS light (blue). The mobile ion simulation demonstrates that, in this parameter regime, the incident light is depleted by SBBS later in time ($\omega_0 t > 12\,000$). The

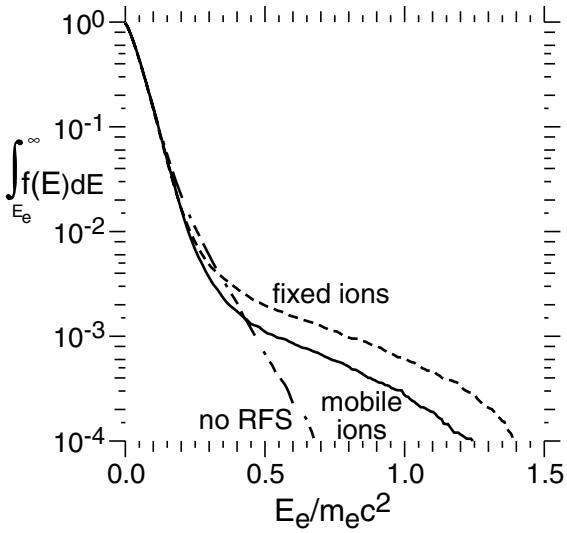

FIG. 3. Electron spectra for $T_e = 20$ keV and $n_e/n_c = 0.2$. Rescatter of the SRFS light by SBBS reduces the hot electron fraction and temperature by reducing the amplitude of the Langmuir wave associated with SRFS.

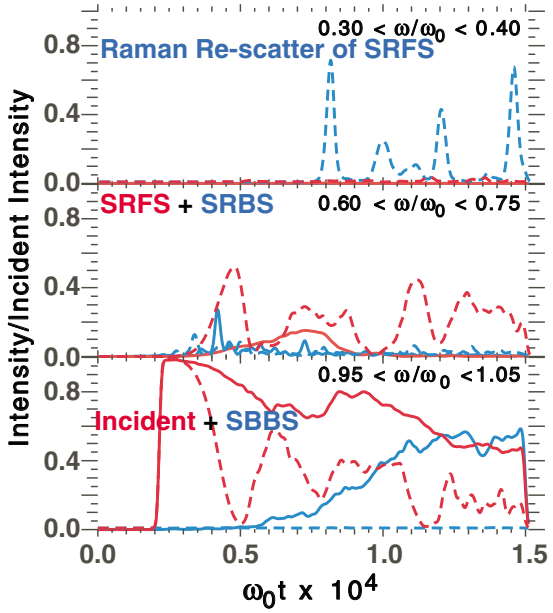

FIG. 4 (color). Normalized intensity vs $\omega_0 t$ for $T_e = 5$ keV and $n_e/n_c = 0.1$. Incident (red) and SBBS (blue) intensities are depicted in the lower panel, SRFS (red) and SRBS (blue) intensities are depicted in the middle panel, and *rescatter of SRFS by SRBS* is depicted in the top panel. Mobile (fixed) ion results are represented by solid (dashed) curves. SRFS saturates by LDI (rescatter) when the ions are mobile (fixed).

middle panel is a plot of intensity in the frequency band $0.60 \leq \omega/\omega_0 \leq 0.75$, which encompasses the SRBS and SRFS light. When the ions are fixed, SRFS depletes the incident light. However, when the ions are mobile, the SRFS light intensity is greatly reduced. Examination of the wave number spectrum indicates that Langmuir decay of the Raman forward-scattered light into a backward-propagating Langmuir wave and an ion acoustic wave depletes the SRFS light. The electron spectrum reveals a dominant feature at $k_L \sim 0.35(\omega_0/c)$, near the back of the simulation box. This is the wave number of the Langmuir waves associated with Raman forward scatter and their decay. In the ion spectrum, there is a feature at $k_{\text{ion}} \sim 0.67(\omega_0/c)$, also near the back of the box. Wave number matching for the Langmuir decay instability occurs, namely, $k_L = k_{\text{ion}} - k_L$.

The top panel in Fig. 4 shows intensity in the frequency band $0.30 \leq \omega/\omega_0 \leq 0.40$ for fixed ions. This backscatter is emitted in short, intense pulses originating at the far end of the plasma, where the SRFS light has reached high levels. This is *Raman rescatter of the SRFS light*; i.e., when the ions are fixed, the SRFS light undergoes Raman rescatter rather than LDI.

In summary, in the HEDS regime, the dominant limiting process for SRFS is rescatter by SBBS. This increases the reflectivity from 15% (just from SRBS with immobilized ions) to over 40% (from a combination of SRBS and rescatter) in our simulations. This rescattering mechanism reduces the fraction of generated hot electrons as well as their temperature.

These findings impact HEDS experimental diagnostics. If the spectrum of SRFS rescatter is misinterpreted as SRBS, one might infer that SRBS is occurring at lower density, $n_e/n_c = 0.15$. Furthermore, fixed ion simulations will overestimate the hot electron temperature and fraction generated by Raman scatter. Ion motion is of consequence in this regime because SBBS of the SRFS light serves to reduce the Langmuir wave amplitude.

Rescatter of SRFS light by SBBS is an important and novel saturation mechanism for plasma at high electron temperature [$T_e > 10$ keV and density ($n_e > 0.1 n_c$)]. In such routinely created plasmas, we see no evidence of LDI of the Langmuir wave associated with SRFS, a finding which corroborates previous analytic estimates for large $k_L \lambda_{de}$ [6]. We do, however, see evidence of LDI of the SRFS Langmuir waves in ignition-type plasmas ($T_e \sim 5$ keV, $n_e \sim 0.1 n_c$), where $k_L \lambda_{de}$ is smaller.

We will further examine suppression of SRFS by density gradients, and its interplay with SRBS, SBBS, and filamentation. We are also performing two-dimensional PIC simulations of a laser hotspot in the HEDS regime to build our multidimensional understanding. Ultimately, we plan to do three-dimensional simulations with Z3 [9], currently under development at LLNL.

We acknowledge invaluable input from L. J. Suter in the design of these targets. This work was performed under the auspices of the U.S. Department of Energy by the University of California Lawrence Livermore National Laboratory under Contract No. W-7405-ENG-48.

[1] J. D. Lindl *et al.* (to be published).
[2] K. G. Estabrook and W. L. Kruer, Phys. Fluids **26**, 1892 (1983).
[3] Brillouin rescatter of Brillouin backscatter has been previously investigated; cf. T. Speziale *et al.,* Phys. Fluids **23**, 1275 (1980).
[4] J. D. Lindl, *Inertial Confinement Fusion* (Springer, New York, 1998), pp. 135–162.
[5] K. L. Baker *et al.,* Phys. Plasmas **6**, 4284 (1999); H. X. Vu, D. F. DuBois, and B. Bezzerides, Phys. Rev. Lett. **86**, 4306 (2001).
[6] D. F. DuBois and M. V. Goldman, Phys. Rev. **164**, 207 (1967); H. X. Vu, D. F. DuBois, and B. Bezzerides, Phys. Plasmas (to be published).
[7] A. B. Langdon and B. F. Lasinski, *Methods in Computational Physics* (Academic Press, New York, 1976), Vol. 16, pp. 327–366.
[8] Related rescattering is also being seen in simulations of longer wavelength laser-plasma interactions; cf. W. L. Kruer, Bull. Am. Phys. Soc. **46**, 286 (2001).
[9] B. F. Lasinski, C. H. Still, and A. B. Langdon, Bull. Am. Phys. Soc. **46**, 203 (2001).